Macromolecular Rapid Communications
www.mrc-journal.de

Theory on Capillary Filling of Polymer Melts in Nanopores

Yang Yao, Hans-Jürgen Butt, George Floudas, Jiajia Zhou, and Masao Doi*

A unified theory for the imbibition dynamics of entangled polymer melting into nanopores is presented. Experiments demonstrate the validity of $t^{1/2}$ dependence but contradict the predictions of the classical Lucas–Washburn equation because of the prefactor. A reversal in dynamics of capillary filling is reported with increasing polymer molecular weight. Polymer imbibition under nanometer confinement can be discussed by two mechanisms: one is the standard hydrodynamic flow, resulting in a parabolic flow profile. When the inner wall has a strong attraction to the polymer, a layer of immobile chains is created, resulting in an increase of the effective viscosity and to slower imbibition. The other is the reptation model proposed by Johner et al., leading to a plug flow profile and to the reduction in the effective viscosity (faster imbibition). The reversal in dynamics of polymer imbibition can be explained by the competition between these two mechanisms.

1. Introduction

Understanding fluid dynamics in a confined geometry is important in many different fields such as engineering, physics, chemistry, biotechnology, and nanotechnology. Successful applications include the development of inkjet printheads for commercial xerography, synthesis and production of various nanoparticles and polymeric materials on a lab-on-a-chip device, separation and manipulation of DNA or other bio-macromolecules, and on-the-spot medical diagnosis in clinical pathology. Under spatial confinement, the volume of the fluid reduces, and the surface-to-volume ratio increases. This leads to the fact that the interaction between the fluid and the surface, i.e., the capillary effect, becomes the dominant factor among many other interactions. A canonical example is the fluid imbibition into a pore with hydrophilic inner surfaces. For Newtonian fluid, the standard model to describe the imbibition dynamics is the celebrated Lucas–Washburn equation (LWE)[1,2]

$$h(t) = At^{1/2},\ A = \sqrt{\frac{R\gamma\cos\theta_E}{2\eta_0}} \tag{1}$$

Here $h(t)$ is the imbibition length of the fluid inside the pore, R is the pore radius, γ is the surface tension of the fluid, θ_E is the equilibrium contact angle, and η_0 is the fluid viscosity in the bulk. The dynamical scaling of $t^{1/2}$ has been found in many phenomena involving capillarity and wetting.[3] Extensive studies by experiments,[4–7] theory,[8,9] and simulations[10–12] have advanced our understanding on the capillary filling, but there are still new avenues to be explored.[13,14]

An implicit assumption in the derivation of Lucas–Washburn equation is that the size of fluid particles should be an order of magnitude smaller than the pore radius. This is valid for simple fluids, for example, when water ($\approx 10^{-10}$ m) fills an µm-size glass pore. Experimentalists nowadays can probe the range where the two length scales are comparable: for example, when a polymer (radius of gyration $R_g \approx 10 - 100$ nm) penetrates into self-ordered nanoporous aluminum oxide (AAO) (also $R \approx 10 - 100$ nm).[13,14] Surprisingly, the dynamical scaling of $t^{1/2}$ is consistently observed in experiments and remains valid in the nanometer ranges. However, the prefactor A exhibits interesting behaviors even for simple liquids.[5] From the experimentally measured A value, one can deduce an effective viscosity

$$\eta_{eff} = \frac{R\gamma\cos\theta_E}{2A^2} \tag{2}$$

The value of η_{eff} is in general different than the bulk value η_0.

Recent experiments have shown a complex behavior of the effective viscosity for capillary imbibition of polymer melts into nanoscale pores.[14] Capillary penetration of a series of entangled poly(ethylene oxide) (PEO) melts within nanopores of self-ordered alumina followed $h \sim t^{1/2}$ behavior according to the LWE. However, a reversal in dynamics of capillary filling has been observed with increasing polymer molecular weight. Polymer chains with 50 entanglements or less showed a slower capillary filling than theoretically predicted, indicating a higher effective viscosity. For longer chains with more entanglements, the capillary filling was faster than the theory and the effective viscosity was reduced as compared to bulk. In this article, we present a possible explanation for this unusual observation.

Y. Yao, Prof. H.-J. Butt, Prof. G. Floudas
Max Planck Institute for Polymer Research
D55128 Mainz, Germany
Prof. J. Zhou
Key Laboratory of Bio-inspired Smart Interfacial Science and Technology of Ministry of Education
School of Chemistry
Beihang University
Beijing 100191, China
E-mail: jjzhou@buaa.edu.cn
Prof. J. Zhou, Prof. M. Doi
Center of Soft Matter Physics & Its Applications
Beihang University
Beijing 100191, China
The ORCID identification number(s) for the author(s) of this article can be found under https://doi.org/10.1002/marc.201800087.

DOI: 10.1002/marc.201800087

 © 2018 WILEY-VCH Verlag GmbH & Co. KGaA, Weinheim

2. Theoretical Considerations

We first present a brief derivation of the Lucas–Washburn equation. Let us consider a cylindrical pore of radius R (schematically shown in **Figure 1**). One end of the pore is in contact with a Newtonian fluid bath, and the fluid is drawn into the pore under capillarity. The dynamics of the filling can be described by $h(t)$, the length of the fluid inside the pore.

There are two opposite forces acting on the fluid.

i) Capillary force

$$F_c = 2\pi R\left(\gamma_{SV} - \gamma_{SL}\right) = 2\pi R\gamma\cos\theta_E \tag{3}$$

where γ_{SV}, γ_{SL}, and γ are the interfacial tension between solid/vapor, solid/fluid, and fluid/vapor, respectively. These three interfacial tensions are related by the Young's relation, $\gamma_{SV} - \gamma_{SL} = \gamma\cos\theta_E$, where θ_E is the equilibrium contract angle. Here we only consider a hydrophilic surface, i.e., $\theta_E < 90°$. The capillary force drives the imbibition.

ii) Viscous force

$$F_v = 8\pi\eta_0 hv \tag{4}$$

where η_0 is the fluid viscosity and $v = \mathrm{d}h/\mathrm{d}t$ is the filling speed. The prefactor depends on the pore geometry, and for circular pore it equals to 8π. The viscous force provides the friction against the imbibition.

The balance between the capillary and viscous forces results in the evolution equation

$$2\pi R\gamma\cos\theta_E = 8\pi\eta_0 hv \tag{5}$$

$$\Rightarrow v = \frac{R\gamma\cos\theta_E}{4\eta_0 h} \tag{6}$$

The solution to the above equation is

$$h^2 = \frac{R\gamma\cos\theta_E}{2\eta_0}t \tag{7}$$

This is the classical Lucas–Washburn Equation (1) with $h \sim t^{1/2}$ scaling.

We would like to point out some general requirements for systems to have the $t^{1/2}$ scaling. The left-hand side of the force balance Equation (5) is a thermodynamic force, which can be derived from conserved potential energy. This term must not depend on h. A counterexample is the capillary rising when gravity is important. In this case, the gravitational force is proportional to the mass of the fluid, and $h(t)$ eventually approaches an asymptotic Jurin's height at long time. The right-hand side of the force balance Equation (5) is related to the energy dissipation. In the simplest form of Equation (4), the force is due to the viscous dissipation resulting from the parabolic flow profile. This term must be proportional to h. A counterexample is the dissipation in the meniscus at the fluid front. In this case, a friction force related to the meniscus has no h-dependency, and the resulting evolution of $h(t)$ would not be of the Lucas–Washburn type ($t^{1/2}$).

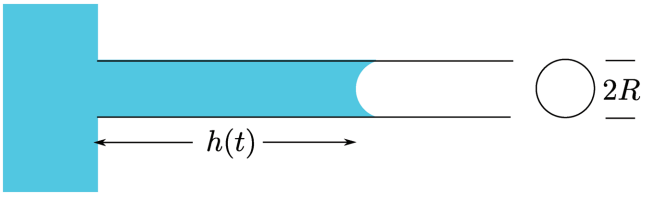

Figure 1. A sketch of fluid imbibition into a cylindrical pore.

In the following, we will consider the imbibition of polymeric fluids into nanopores. We focus on the situation where the Lucas–Washburn scaling $t^{1/2}$ is valid, and consider various effects that may lead to different prefactors in a modified LWE.

2.1. Confinement Effect

When the pore diameter is of the same order as the molecule size, as in our case of polymeric fluids, the conformation of the polymer chain is perturbed. In general, polymer chains have higher free energy in the pores than in the bulk. This reduces the driving force for the filling, and may be described by an effective surface tension

$$\gamma_{eff} = \gamma\cos\theta_E - \Delta f\frac{R}{2} \tag{8}$$

where Δf is the change in the free energy density of a polymer melt under confinement in comparison to the bulk.

We may evaluate Δf using the blob model.[15] The polymer chains are under biaxial confinement and can be viewed as a sequence of compression blobs of the pore diameter $2R$. For ideal chains, the number of monomer g in each compression blob is given by $g = (2R/b)^2$, where b is the statistical length of the monomer (Kuhn length). The number of blobs per chain is given by N/g, where N is the number of monomers per chain. The free energy penalty due to confinement is of the order of k_BT per compression blob, i.e., $\Delta F = k_BT\,N/g = k_BT\,Nb^2/(4R^2)$. To obtain the free energy density, we use the number density of the polymer chain $1/(v_0N)$, where v_0 is the monomer volume. The difference in the free energy density Δf is then given by

$$\Delta f = \frac{1}{v_0 N}\times k_BT\frac{Nb^2}{4R^2} = k_BT\frac{b^2}{4v_0R^2} \tag{9}$$

We estimate the effect of confinement by comparing the two terms in Equation (8). The ratio between these two terms is

$$\frac{k_BT}{\gamma\cos\theta_E}\frac{b^2}{8v_0R} \tag{10}$$

Using the experiments of PEO in AAO pores as an example[14]: $v_0 = 6.04\times10^{-29}$ m^3, $T = 358$ K, $k_BT = 4.94\times10^{-21}$ J, $\gamma\cos\theta_E = 0.02$ J m^{-2}, $b = 0.68$ nm, and $2R = 35$ nm, this results a ratio of 0.014. This is too small an effect to account for the increase in the effective viscosity. Note here we considered the confinement energy based on an isolated ideal chain. For the melt system, this energy is due to the

© 2018 WILEY-VCH Verlag GmbH & Co. KGaA, Weinheim

fluctuation-induced long-range interaction and was shown to be even smaller [b/R of Equation (9)].[16,17]

2.2. Dead Zone Effect

For simple fluids, the flow profile inside the pore has a parabolic profile, a result of the Stokes equation and no-slip boundary condition on the wall. For polymeric fluids, the polymer chains near the inner wall can be strongly adsorbed. There exist experimental evidences for that from dielectric spectroscopy measurements for polymers confined to nanoporous alumina.[18] These immobile chains create a "dead zone" of thickness ΔR. We define an effective radius of the pore by $R_{\text{eff}} = R - \Delta R$, and consider the effect of dead zone on the imbibition speed.

Outside the dead zone, the polymer melts exhibit a macroscopic flow with the usual parabolic profile. We rewrite Equation (6) in term of a pressure

$$v = \frac{R^2}{8\eta_0 h}\Delta P, \quad \Delta P = \frac{2\gamma\cos\theta_{\text{E}}}{R} \tag{11}$$

where ΔP is the Laplace pressure that drives the imbibition. This term remains unchanged when the dead zone is considered, but we have to replace R^2 in the numerator by R_{eff}^2. Since only R_{eff}^2/R^2 portion of the polymer contributes to the flow, the fluid front advances at the rate

$$\dot{h} = v\frac{R_{\text{eff}}^2}{R^2} = \frac{R_{\text{eff}}^4}{8\eta_0 h R^2}\Delta P = \frac{R_{\text{eff}}^4}{8\eta_0 h R^2}\frac{2\gamma\cos\theta_{\text{E}}}{R} \tag{12}$$

Comparing the above equation to Equation (6) with η_0 replaced by an effective viscosity η_{eff}, defined by $\dot{h} = \gamma\cos\theta_E R/(4\eta_{\text{eff}} h)$, we obtain the following expression for η_{eff}

$$\frac{\eta_{\text{eff}}}{\eta_0} = \left(\frac{R}{R_{\text{eff}}}\right)^4 \tag{13}$$

Since $R_{\text{eff}} < R$, we have $\eta_{\text{eff}} > \eta_0$. Also because of the fourth power, the effect of dead zone is quite substantial even for a small change in R_{eff}. This is the origin of the slow-down in the imbibition dynamics for shorter chains.

2.3. Reptation under Confinement

As the pore radius is reduced and becomes comparable to the thickness of the dead zone, the macroscopic flow is nearly stopped. The material transport under very strong confinement is achieved mainly by the reptation of free polymer chains in a network driven by the pressure gradient. Johner et al. has developed a theoretic framework for this scenario.[8] Here we present their results for completeness, while also include the pore-size dependence of the pressure gradient.

Figure 2 shows one single free chain under a pressure gradient. A polymer chain is constrained by other chains due to entanglements, and as such it can only move along the "reptation tube". Each free polymer chain experiences a driving force due to the pressure difference along the chain

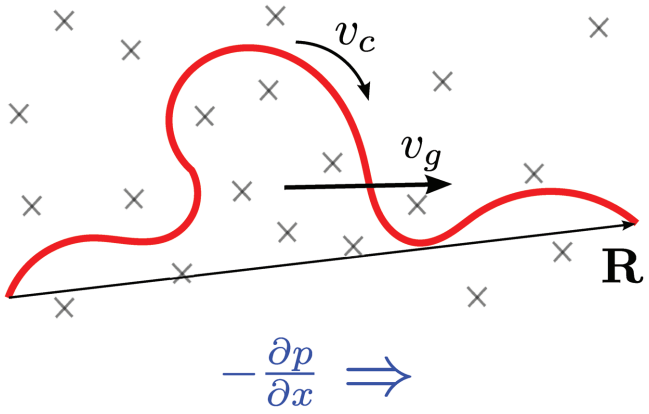

Figure 2. Schematics of reptation motion of a polymer chain under a pressure gradient.

$[-p(x+R_x) + p(x)]\,\ell^2 = -\ell^2 R_x \partial p/\partial x$, where ℓ^2 is the cross section and R_x is the x-component of the end-to-end vector. The friction to the free chain is given by $N\zeta v_c$, where N is number of segments, ζ is the friction constant for one Kuhn segment, and v_c is the chain's velocity along the reptation tube. The balance between the pressure gradient and the frictional force gives

$$v_c = \frac{\ell^2}{\zeta N}R_x\left(-\frac{\partial p}{\partial x}\right) \tag{14}$$

The averaged velocity for the center of mass of the polymer is

$$\langle v_g\rangle = \left\langle\frac{R_x}{L}v_c\right\rangle = \frac{\ell^2}{\zeta NL}\langle R_x^2\rangle\left(-\frac{\partial p}{\partial x}\right) = \frac{\ell^2 a_t}{3\zeta N}\left(-\frac{\partial p}{\partial x}\right) \tag{15}$$

where L is the contour length of the tube, given by $L = (N/N_e)a_t$. N_e is the entanglement length and $a_t = \sqrt{N_e}\,b$ is the tube diameter. The average of R_x^2 is assumed to be ideal $\langle R_x^2\rangle = (1/3)Nb^2$.

If the fraction of polymer chains participating the reptation is φ, the filling speed is then given by

$$\dot{h} = \varphi\langle v_g\rangle = \varphi\frac{\ell^2 a_t}{3\zeta N}\frac{2\gamma\cos\theta_{\text{E}}}{hR} \tag{16}$$

where we averaged the pressure gradient along the whole fluid, $-\partial p/\partial x = \Delta P/h = 2\gamma\cos\theta_{\text{E}}$.

Complication arises when one needs to specify the cross-section ℓ^2. One natural choice is the cross-section of the reptation tube

$$\ell^2 = a_t^2 \Rightarrow \dot{h} = \varphi\frac{N_e^{3/2}b^3}{3\zeta N}\frac{2\gamma\cos\theta_{\text{E}}}{hR} \tag{17}$$

In reference [8], Johner et al. used

$$\ell^2 = \frac{N_e b^3}{\sqrt{N_e}\,b} = N_e^{1/2}\,b^2 \Rightarrow \dot{h} = \varphi\frac{N_e b^3}{3\zeta N}\frac{2\gamma\cos\theta_{\text{E}}}{hR} \tag{18}$$

The only difference is in the scaling with respect to N_e. Here we shall assume a general form of

© 2018 WILEY-VCH Verlag GmbH & Co. KGaA, Weinheim

$$\dot{h} = \varphi \frac{N_e^{\alpha} b^3}{3\zeta N} \frac{2\gamma \cos\theta_E}{hR} \tag{19}$$

where α is the exponent.

2.4. Summary on Effective Viscosity

In the case of $R_g << R$, the dead-zone effect is dominant and the filling dynamics is given by Equation (12). In the other limit, $R_g >> R$, the reptation mode is important and the filling dynamics is governed by Equation (19). A simple formula to interpolate these two limits is

$$\dot{h} = \left[\frac{R_{eff}^4}{8\eta_0 R^2} + \varphi \frac{N_e^{\alpha} b^3}{3\zeta N} \right] \frac{2\gamma \cos\theta_E}{hR} \tag{20}$$

We again define an effective viscosity by

$$\dot{h} = \frac{\gamma \cos\theta_E R}{4\eta_{eff} h} = \frac{R^2}{8\eta_{eff}} \frac{2\gamma \cos\theta_E}{hR} \tag{21}$$

Comparing the above two equations, we obtain

$$\frac{\eta_{eff}}{\eta_0} = \left[\left(\frac{R_{eff}}{R} \right)^4 + \phi \frac{8 N_e^{\alpha} b^3 \eta_0}{3\zeta N R^2} \right]^{-1} \tag{22}$$

In the limit of small pore, the first term in the square bracket vanishes because $R_{eff} \to 0$. The effective viscosity is then dominant by the second term

$$\eta_{eff} \sim \eta_0 \left(\frac{\eta_0}{N} \right)^{-1} \sim N^1 \tag{23}$$

This is quite different than the bulk scaling $\eta_0 \sim N^3$. Thus confined polymers show an enhanced mobility, consistent with the experiment findings in references [13,14] that have shown exponents of ≈ 1.4 and ≈ 0.9, respectively.

3. Comparison to the Experiment and Discussion

We compare our theoretical model with the capillary filling experiments in reference [14]. The bulk properties of PEO melts of different molecular weights are shown in **Table 1**. A fit to the viscosity gives $\eta_0 \sim N^{2.91}$, which indicates that we may use the standard formulation of Doi–Edwards model[19]

Table 1. PEO melt properties.

Sample	γ [10^{-3} N m^{-1}]	θ_E [°]	η_0 [Pa s]
PEO 50k	29.1	44.0	4.3×10^2
PEO 100k	27.8	44.5	3.9×10^3
PEO 280k	28.0	44.0	1.5×10^5
PEO 500k	28.1	40.7	4.6×10^5
PEO 1M	28.0	47.7	2.7×10^6

$$\eta_0 \approx \frac{\zeta b^2}{v_0} \frac{N^3}{N_e^2} \tag{24}$$

The effective viscosity in Equation (22) can be rewritten as

$$\frac{\eta_{eff}}{\eta_0} = \left[f(\Delta R, R) + g(\phi, N, R) \right]^{-1} \tag{25}$$

The first function f is related to the dead-zone

$$f(\Delta R, R) = \begin{cases} \left(1 - \dfrac{\Delta R}{R}\right)^4 & \text{if } R > \Delta R \\ 0 & \text{if } R < \Delta R \end{cases} \tag{26}$$

The second function g is from the reptation model

$$g(\phi, N, R) = \varphi \frac{8 N_e^{\alpha} b^3}{3\zeta} \frac{\eta_0}{NR^2} = \varphi \frac{8 N_e^{\alpha-2} b^5}{3 v_0} \frac{N^2}{R^2} = \phi \frac{N^2}{R^2} \tag{27}$$

where we have used Equation (24) and grouped parameters into one single factor ϕ. In the end, we have two free parameters: ΔR and ϕ. In principle, these two parameters may vary for different pore radii and molecular weights. As a first attempt, we neglect that dependence and assume ΔR and ϕ are constants.

Figure 3 shows the comparison between the experiment and theory. We plot the ratio of the effective viscosity to the bulk viscosity as a function of $1/R$, the inverse of the pore radius, for a polymer with various molecular weights. The fitting parameters are obtained by global fitting resulting to

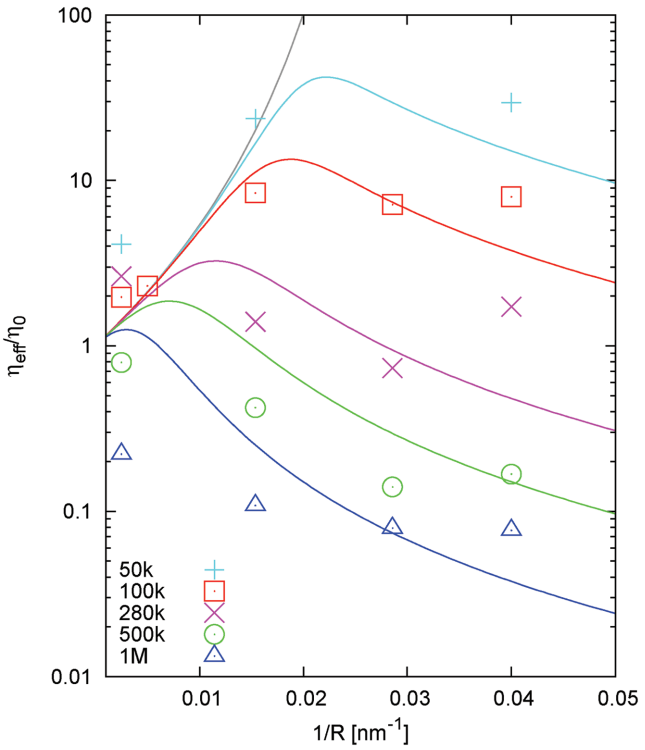

Figure 3. Comparison between the experiment and the theory. The symbols are shown for the experimental data taken from reference [14]. The lines are from theoretical prediction of Equation (25).

© 2018 WILEY-VCH Verlag GmbH & Co. KGaA, Weinheim

$$\Delta R = 34.3\ \text{nm}, \quad \phi = 3.21\times 10^{-5}\left[\text{nm}^2\right] \tag{28}$$

The theoretic prediction is in qualitative agreement with the experimental data. Most importantly, the theory has captured the non-monotonic variation in the effective viscosity. The main reason for the non-monotonic behavior is that functions f and g vary differently with respect to $1/R$. In the large pore limit, these two functions $f \to 1$ while $g \to 0$, and the effective viscosity approaches the bulk value, $\eta_{\text{eff}} \to \eta_0$. As the pore radius decreases ($1/R$ increases), the effect of the dead zone becomes important and eventually stops the macroscopic flow. Accordingly, the function f decreases. On the other hand, for small pores the reptation motion of the entangled polymer becomes effective and function g increases. It is the opposite trends in the functions f and g that lead to the non-monotonic variation of the effective viscosity as observed experimentally.

The inversion point, i.e., the value of $1/R$ when the effective viscosity has its maximum, is a function of the molecular weight. For polymers of low molecular weight, the inversion point corresponds to a pore radius that is comparable with the thickness of the dead-zone, ΔR. Alternatively, for longer chains, the maximum shifts towards $1/R \to 0$, i.e., to the very weak confinement limit.

4. Summary

We present a theoretical model for the imbibition dynamics of entangled polymer melts into nanopores. Experiments have demonstrated the validity of the $t^{1/2}$ scaling, however the Lucas–Washburn equation breaks down because of the prefactor. We have considered various effects that can affect the imbibition dynamics while preserving the $t^{1/2}$ scaling:

i) The effect of confinement. Biaxial confinement of polymer chains induces a penalty in the free energy, but the effect is too small to explain the slow-down in dynamics.
ii) The effect of adsorption. Strongly-adsorbed chains create a dead zone, reducing the pore radius, and leading to an increase in the effective viscosity.
iii) The effect of reptation under a pressure gradient: The reptation of polymer chains under strong confinement[8] enhances the mobility of confined chains, leading to faster imbibition.

The overall imbibition dynamics can be discussed by the competition of the latter two mechanisms. The theoretical predictions capture the main features of the experiment being in a qualitative agreement with the experiments.

Note: We recently demonstrated a very interesting imbibition behavior for binary mixture of polymer chains [https://doi.org/10.1021/acs.macromol.7b02724].

Acknowledgements

The work in Beihang University was supported by the National Natural Science Foundation of China (NSFC) through the Grants No. 21504004 and 21774004. M.D. acknowledges the financial support of the Chinese Central Government via the Thousand Talents Program.

Conflict of Interest

The authors declare no conflict of interest.

Keywords

capillary filling, confinement, polymer melts, reptation

Received: January 30, 2018
Revised: March 22, 2018
Published online: April 24, 2018

[1] R. Lucas, *Kolloid-Z.* **1918**, *23*, 15.
[2] E. W. Washburn, *Phys. Rev.* **1921**, *17*, 273.
[3] P.-G. de Gennes, F. Brochard-Wyart, D. Quéré, *Capillarity and Wetting Phenomena*, Springer, New York, USA **2004**.
[4] S. Ok, M. Steinhart, A. Sterbescu, C. Franz, F. V. Chávez, K. Saalwächter, *Macromolecules* **2010**, *43*, 4429.
[5] F. Chauvet, S. Geoffroy, A. Hamoumi, M. Prat, P. Joseph, *Soft Matter* **2012**, *8*, 10738.
[6] L. Mammen, P. Papadopoulos, K. Friedemann, S. Wanka, D. Crespy, D. Vollmer, H.-J. Butt, *Soft Matter* **2013**, *9*, 9824.
[7] B.-Y. Cao, M. Yang, G.-J. Hu, *RSC Adv.* **2016**, *6*, 7553.
[8] A. Johner, K. Shin, S. Obukhov, *Europhys. Lett.* **2010**, *91*, 38002.
[9] N.-K. Lee, D. Diddens, H. Meyer, A. Johner, *Phys. Rev. Lett.* **2017**, *118*, 067802.
[10] D. I. Dimitrov, A. Milchev, K. Binder, *Phys. Rev. Lett.* **2007**, *99*, 054501.
[11] M. R. Stukan, P. Ligneul, J. P. Crawshaw, E. S. Boek, *Langmuir* **2010**, *26*, 13342.
[12] W. Stroberg, S. Keten, W. K. Liu, *Langmuir* **2012**, *28*, 14488.
[13] K. Shin, S. Obukhov, J.-T. Chen, J. Huh, Y. Hwang, S. Mok, P. Dobriyal, P. Thiyagarajan, T. P. Russell, *Nat. Mater.* **2007**, *6*, 961.
[14] Y. Yao, S. Alexandris, F. Henrich, G. Auernhammer, M. Steinhart, H.-J. Butt, G. Floudas, *J. Chem. Phys.* **2017**, *146*, 203320.
[15] M. Rubinstein, R. H. Colby, *Polymer Physics*, Oxford University Press, Oxford, UK **2003**.
[16] A. N. Semenov, S. P. Obukhov, *J. Phys.: Condens. Matter* **2005**, *17*, S1747.
[17] N.-K. Lee, J. Farago, H. Meyer, J. P. Wittmer, J. Baschnagel, S. P. Obukhov, A. Johner, *Europhys. Lett.* **2011**, *93*, 48002.
[18] S. Alexandris, G. Sakellariou, M. Steinhart, G. Floudas, *Macromolecules* **2014**, *47*, 3895.
[19] M. Doi, S.F. Edwards, *The Theory of Polymer Dynamics*, Oxford, UK **1994**.

© 2018 WILEY-VCH Verlag GmbH & Co. KGaA, Weinheim